Available online at www.sciencedirect.com
SCIENCE DIRECT®
Thermochimica Acta 432 (2005) 10–19
thermochimica acta
www.elsevier.com/locate/tca

Evaluation of the parameters of the Bender equation of state for low acentric factor fluids and carbon dioxide

J. Ghazouani, O. Chouaieb, A. Bellagi*

U.R.: Thermique et Thermodynamique des Procédés Industriels, Ecole Nationale d'Ingénieurs de Monastir, ENIM, Av. Ibn Jazzar, 5060 Monastir, Tunisia

Received 26 June 2004; received in revised form 19 October 2004; accepted 1 November 2004
Available online 10 May 2005

Abstract

Volumetric properties of several low acentric factor fluids (Ar, CH_4, C_2H_6, Kr, N_2, Ne, O_2, Xe) as well as CO_2 are modeled using the Bender equation of state. This equation is a linear function of 19 adjustable parameters, which are evaluated from properties data, using a linear numerical procedure. The validity of the EOS is tested by calculating the Joule–Thomson inversion curve. A simple model is in particular used to correlate the inversion properties predicted by the Bender equation, expressed in term of reduced pressure as a function of reduced temperatures ranging from 0.8 to 6. The simple correlation reproduces accurately the used data. We employ data on state behaviour $\rho(P, T)$ of homogeneous fluid phases, vapour–liquid equilibrium, second virial coefficient and the coordinates of the critical point.

Keywords: Equation of state; Second virial coefficient; Inversion curve; Acentric factor; Pure fluids

1. Introduction

The Bender equation of state [1], with 19 adjustable parameters, constitutes a good compromise between common simple equations and more elaborated equations. It can reproduce with high fidelity the properties of the fluids in a wide area of the thermodynamic surface, in both homogeneous fluid regions as well as at the vapour–liquid equilibrium curve. The Bender equation is generally written in terms of the compressibility factor Z as a function of temperature T and density ρ:

$$Z = PM/RT\rho = 1 + B\rho/R + C\rho^2/R + D\rho^3/R + E\rho^4/R + F\rho^5/R + (G + H\rho^2)\rho^2/R\,\mathrm{e}^{-\rho^2/a_{20}^2} \quad (1)$$

where

$$B = a_1 + a_2/T + a_3/T^2 + a_4/T^3 + a_5/T^4,$$
$$C = a_6 + a_7/T + a_8/T^2, \qquad D = a_9 + a_{10}/T,$$
$$E = a_{11} + a_{12}/T, \qquad F = a_{13}/T,$$
$$G = a_{14}/T^3 + a_{15}/T^4 + a_{16}/T^5,$$
$$H = a_{17}/T^3 + a_{18}/T^4 + a_{19}/T^5. \quad (2)$$

If a_{20} is set as usual equal to ρ_c, Eq. (1) is a linear function of the 19 adjustable fluid specific parameters which can be evaluated from properties data using a numerical fitting methods like that proposed by Cibulka et al. [2]. The validity of the equation is tested in the present paper not only by comparing the calculated volumetric properties with their data values but also by comparing the Joule–Thomson inversion curve predicted by the Bender equation with published inversion data. We show the importance of incorporating a derivative property like the second virial coefficient for the correct evaluation of the adjustable parameters. We consider in this paper only the low acentric factor fluids (Ar, CH_4, C_2H_6, Kr, N_2, Ne, O_2, Xe) as well as CO_2. Table 1 gives the main characteristics of the considered fluids i.e., the critical data T_c, P_c and Z_c, the Pitzer acentric factor ω and the Boyle temperature T_B.

* Corresponding author. Tel.: +216 73500244; fax: +216 73500514.
E-mail address: a.bellagi@enim.rnu.tn (A. Bellagi).

0040-6031/$ – see front matter © 2004 Elsevier B.V. All rights reserved.
doi:10.1016/j.tca.2004.11.008

Table 1
Characteristics of the considerd fluids

Fluid	T_c (K)	P_c (kPa)	Z_c	w [3]	T_B (K)
Ar	150.687	4863.0	0.2895	−0.00219	408
CH_4	190.564	4599.2	0.2863	0.01142	508
C_2H_6	305.33	4871.8	0.2788	0.0993	747
Kr	209.48	5510.0	0.2918	−0.001714	579
Ne	44.4918	2678.6	0.3032	−0.0387	119
N_2	126.192	3395.8	0.2894	0.0372	327
O_2	154.581	5043.0	0.2879	0.0222	405
Xe	289.734	5840.0	0.2893	0.00363	798
CO_2	304.1282	7377.3	0.2746	0.22394	722

2. Data sources

The (ρ, P, T) properties of the pure fluids, used in the following fitting procedure, are taken from the NIST compilation [3]. In particular, we used the following state data:

- gas phase: $Z(T, \rho)$;
- liquid phase: $Z(T, \rho)$;
- vapour–liquid equilibrium: $P_{sat}(T)$, $\rho_{sat}^{(G)}(T)$, $\rho_{sat}^{(L)}(T)$;
- gas–liquid critical point: (Z_c, T_c, ρ_c).

The second virial coefficients are calculated either with their most recent equations of state as given in [4]: Ar [5], CH_4 [6], C_2H_6 [7], Ne [8], N_2 [9], O_2 [10] and CO_2 [11] or taken from the compilation in [12] (Kr, Xe).

Tables 2 and 3 give the ranges of used data groups and the number of data points for each substance.

3. Numerical procedure

The proposed method is based on the minimization of the sum of the pondered quadratic residues, ϕ_K, of the individual data groups (K is: G for gas; L for liquid; VLE for vapour–liquid equilibrium; V for second virial coefficient) as objective function Ψ of the parameters vector $\mathbf{a} = (a_1, \ldots, a_{19})$:

$$\Psi(\mathbf{a}) = w_G\phi_G + w_L\phi_L + w_{VLE}\phi_{VLE} + w_V\phi_V \quad (3)$$

where

$$\phi_G = \sum_{i=1}^{n_{vap}} [Z_i^{(G)} - Z_i^{(cal)}(\mathbf{a}, T_i, \rho_i^{(G)})]^2 \quad (4)$$

$$\phi_L = \sum_{j=1}^{n_{liq}} [Z_j^{(L)} - Z_j^{(cal)}(\mathbf{a}, T_j, \rho_j^{(L)})]^2 \quad (5)$$

$$\phi_{VLE} = \sum_{k=1}^{n_{sat}} \{[(P^{(cal)}(\mathbf{a}, \rho_{sat,k}^{(L)}, T_k) - P_{sat}(T_k))/P_{sat}(T_k)]^2 + [(P^{(cal)}(\mathbf{a}, \rho_{sat,k}^{(G)}, T_k) - P_{sat}(T_k))/P_{sat}(T_k)]^2 + \phi_M^2\} \quad (6)$$

ϕ_M is the Maxwell criterion at the vapour–liquid equilibrium:

$$\phi_M = \sum_{k=1}^{n_{sat}} \left\{ \int_{\rho_{sat}^G}^{\rho_{sat}^L} (Z^{(cal)}(\mathbf{a}, T_{sat,k}, \rho)/\rho)\, d\rho - (Z^{(cal)}(\mathbf{a}, T_{sat,k}, \rho_{sat,k}^{(G)}) - Z^{(cal)}(\mathbf{a}, T_{sat,k}, \rho_{sat,k}^{(L)})) \right\}. \quad (7)$$

Table 2
Ranges of data groups and number of data values for each considered substance

Fluid	Data group	Range of T (K)	Range of P (kPa)	Number of values
Ar	G-data	85–700	8–100000	3584
	L-data	85–150	800–100000	328
	VLE-data	84–150	70.447–4734.6	34
	V-data	84–700		125
CH_4	G-data	100–600	8–100270	1530
	L-data	100–190	2375–100000	469
	VLE-data	100–190	34.376–4518.6	43
	V-data	100–600		101
C_2H_6	G-data	180–625	8–70000	1715
	L-data	180–305	1000–70000	523
	VLE-data	179–305	74.330–4837.8	43
	V-data	180–800		125
Kr	G-data	116–800	8–100000	3896
	L-data	116–206	800–100000	440
	VLE-data	116–209	74.624–5443.4	46
	V-data	116–800		138
N_2	G-data	64–2000	8–100000	9897
	L-data	64–124	800–100000	308
	VLE-data	64–126	14.602–3364.5	59
	V-data	64–2000		391
Ne	G-data	25–700	8–100000	3691
	V-data	25–700		136
O_2	G-data	80–1000	8–82000	4818
	L-data	80–150	800–82000	360
	VLE-data	80–154	30.123–4930.7	66
	V-data	80–1000		185
Xe	G-data	162–800	8–100000	3528
	L-data	162–287	800–100000	635
	VLE-data	162–289	84.849–5752.4	63
	V-data	162–850		140
CO_2	G-data	217–1100	8–100000	5576
	L-data	217–302	1000–100000	445
	VLE-data	217–304	527.22–7355.5	45
	V-data	217–1100		179

The last term in Eq. (3) takes into account the residues of the second virial coefficients:

$$\phi_V = \sum_{l=1}^{n_V} [B_V(T_l) - B_V^{(cal)}(\mathbf{a}, T_l)]^2. \quad (8)$$

Group weight factors w_i are used in Eq. (3) for balancing mutual weights among the different data sets ($K = G, L$, VLE, V). They are calculated in the same manner as in [2].

Four constraints are imposed on the minimum of Ψ: the three usual conditions at the critical point, constraints f_1, f_2 and f_3:

$$f_1 = [Z(\mathbf{a}, T_c, \rho_c) - Z_c] = 0 \quad (9)$$

$$f_2 = \{\partial P(\mathbf{a}, T, V)/\partial V\}_{T,CP} = 0 \quad (10)$$

$$f_3 = \{\partial^2 P(\mathbf{a}, T, V)/\partial V^2\}_{T,CP} = 0 \quad (11)$$

and that of the Boyle temperature T_B

$$f_4 = B_V(\mathbf{a}, T_B) = 0. \quad (12)$$

The optimization problem is now stated as follows

$$\left\{ \begin{array}{c} \min \Psi(\mathbf{a}) \\ f_m(\mathbf{a}) = 0, \quad m = 1, \ldots, 4 \end{array} \right\}. \quad (13)$$

Using the Lagrangian multipliers method with the four multipliers λ_1, λ_2, λ_3 and λ_4 for the four constraints, we obtain a system of 19 equations in 23 unknowns

$$d\Psi(\mathbf{a}) + \sum_{m=1,4} \lambda_m \, d f_m(\mathbf{a}) = 0. \quad (14)$$

The missing 4 equations are the imposed constraints (Eqs. (9)–(12)).

In order to investigate the influence of the individual data groups on the predictive quality of the EOS, we write the objective function Ψ in the form

$$\Gamma(\mathbf{a}, \lambda) = \alpha_G w_G \phi_G + \alpha_L w_L \phi_L + \alpha_{VLE} w_{VLE} \phi_{VLE} + \alpha_V w_V \phi_V + \alpha_{CP}\{\lambda_1 f_1 + \lambda_2 f_2 + \lambda_3 f_3\} + \alpha_B \lambda_4 f_4 \quad (15)$$

By affecting values 1 or 0 to the coefficients α_K, a particular data group may be retained in ($\alpha_K = 1$) or rejected from ($\alpha_K = 0$) the calculations. Several combinations of data groups with various vectors $\{\alpha_K\}$, ($K = G, L$, VLE, V, CP, B) are considered.

The set of linear equations can be rearranged and written in matrix form as

$$\beta \mathbf{X} = \gamma \quad (16)$$

with

$$\mathbf{X} = \{a_1, a_2, \cdots a_{19}, \lambda_1, \lambda_2, \lambda_3, \lambda_4\}^T \quad (17)$$

and

$$\beta = \begin{pmatrix} \beta_{1,1} & \cdots & \beta_{1,23} \\ \vdots & & \vdots \\ \beta_{23,1} & \cdots & \beta_{23,23} \end{pmatrix}, \qquad \gamma = (\gamma_1, \cdots\cdots \gamma_{23})^T \quad (18)$$

The vector $\mathbf{X}$ (Eq. (17)) is found by solving numerically Eq. (16) using the Harwell subroutine MA29D [14] for a symetric β matrix [15]. (Tables 3–5)

To test the predictive capability of the Bender equation for the description of the vapour–liquid equilibrium, we compare the saturation properties ($P_{sat,cal}$, $\rho^{(G)}_{sat,cal}$, $\rho^{(L)}_{sat,cal}$) at a selected temperature T as calculated by solving the set of the two non-linear equations with the resulting parameters $\mathbf{a} = \{a_i\}$:

$$P(\mathbf{a}, T, \rho^{(G)}_{sat,cal}) = P(\mathbf{a}, T, \rho^{(L)}_{sat,cal}) \quad (19)$$

Table 3
Results of selected vectors $\{\alpha_K\}$ for nitrogen[a]

α_i						G		L		VLE		V		CP
G	L	VLE	V	CP	B	$\partial_r Z$ (%)	∂Z	$\partial_r Z$ (%)	∂Z	$\partial_r P_L$ (%)	$\partial_r P_G$ (%)	$\partial_r B_V$ (%)	∂B_V ($m^3\,mol^{-1}$)	$\partial_r Z_c$ (%)
All data														
1	1	1	1	1	1	0.29	0.003	0.52	0.002	0.61	0.24	5.75	0.001	0
G-data														
1	0	0	0	0	0	0.06	0.000	***	0.637	***	0.57	6.33	0.001	4.11
1	1	0	0	0	0	0.11	0.001	0.32	0.000	10.74	1.42	11.20	0.002	−8.28
1	1	1	0	0	0	0.23	0.002	0.40	0.002	0.52	0.17	19.90	0.002	−0.71
1	1	1	1	0	0	0.24	0.003	0.4	0.002	0.55	0.09	7.73	0.001	−1.17
1	1	1	1	0	1	0.26	0.003	0.44	0.002	0.55	0.10	4.48	0.001	−1.29
1	1	1	0	1	0	0.23	0.002	0.33	0.001	0.50	0.27	30.71	0.003	0
L-data														
0	1	0	0	0	0	83.19	0.982	0.07	0.000	0.41	53.51	***	0.641	30.86
0	1	1	0	0	0	3.71	0.042	0.18	0.000	0.53	0.08	***	0.045	0.39
1	1	0	0	1	0	0.30	0.001	0.63	0.001	0.72	0.31	10.51	0.001	0
VLE-data														
0	0	1	0	0	0	17.23	0.227	78.96	1.218	0.04	0.01	***	0.092	0.19
0	0	1	0	1	0	23.81	0.318	92.89	1.553	0.09	0.04	***	0.104	0

Values of deviations equal to or more than 100% are denoted by ***.

Table 4
Confidence intervals and standard error for each parameter of the Bender EOS in the case of nitrogen for the fit with $\alpha = \{1, 0, 0, 0, 0, 0\}$

Parameters	Estimate	CI	S.E.
$a_1 \times 10^3$	9.66475	9.60608; 9.67258	0.00001
a_2	−0.242837	−0.315011; −0.219469	0.02437
$a_3 \times 10^{-2}$	−12.3958	−12.4736; −12.1351	8.63436
$a_4 \times 10^{-4}$	12.0759	11.6828; 12.1928	1301.01
$a_5 \times 10^{-6}$	−4.83593	−4.89985; −4.64306	65501.6
$a_6 \times 10^5$	1.3997	1.38824; 1.45372	1.67035×10^{-7}
$a_7 \times 10^4$	−6.15479	−8.41118; −1.135	0.00019
a_8	−0.194958	−0.200924; −0.18034	0.00525
$a_9 \times 10^9$	−7.60305	−9.31186; −7.0441	5.7845×10^{-10}
$a_{10} \times 10^5$	1.060184	0.864239; 1.15428	7.3982×10^{-7}
$a_{11} \times 10^{11}$	2.79557	2.75756; 2.97717	5.6018×10^{-13}
$a_{12} \times 10^8$	−1.61611	−1.75178; −1.37629	9.5777×10^{-10}
$a_{13} \times 10^{11}$	1.50808	1.4038; 1.56836	4.1976×10^{-13}
$a_{14} \times 10^{-2}$	−2.30933	−2.35535; −2.18602	14.522
$a_{15} \times 10^{-4}$	10.05986	9.78314; 11.0648	3269.3
$a_{16} \times 10^{-5}$	−85.49781	−91.8327; −83.564	210915
$a_{17} \times 10^4$	−4.30436	−5.27453; −2.77599	0.00006
a_{18}	0.137114	0.092618; 0.161308	0.01752
a_{19}	−0.192710	−0.2193113; −0.187131	0.0250

$R^2 = 0.999982$.

$$\phi_M = 0 \tag{20}$$

with the saturation data. The solution of the set of Eqs. (19) and (20) is obtained by means of a non-linear procedure [16].

Table 5
Parameters of the Bender equation of state of nitrogen for selected vectors $\{\alpha_K\}$

α_G	1	1	1
α_L	0	1	1
α_{VLE}	0	1	1
α_V	0	0	0
α_{CP}	0	0	1
α_B	0	0	0
$a_1 \times 10^2$	0.9665	1.0132	1.0052
a_2	−0.2428	−1.7775	−1.3923
$a_3 \times 10^{-2}$	−12.3958	−3.4055	−3.5533
$a_4 \times 10^{-4}$	12.0759	−0.8036	−1.0208
$a_5 \times 10^{-5}$	−48.3594	1.9298	2.2115
$a_6 \times 10^5$	1.3997	2.0374	1.9125
$a_7 \times 10^3$	−0.6155	−8.0088	−9.2313
a_8	−0.1949	0.3743	0.4509
$a_9 \times 10^9$	−7.6030	−9.3718	−5.8968
$a_{10} \times 10^5$	1.0602	2.1536	2.1982
$a_{11} \times 10^{11}$	2.7956	4.8521	4.9045
$a_{12} \times 10^8$	−1.6161	−3.6394	−3.6235
$a_{13} \times 10^{11}$	1.5081	2.4310	2.3827
$a_{14} \times 10^{-2}$	−2.3093	0.1048	−0.0845
$a_{15} \times 10^{-4}$	10.0598	0.9865	1.2281
$a_{16} \times 10^{-5}$	−85.4978	−6.5933	−7.4913
$a_{17} \times 10^4$	−4.3043	−3.191	−3.9388
a_{18}	0.1371	0.1084	0.1300
a_{19}	−0.1927	−0.4338	−0.8534
a_{20}	ρ_c	ρ_c	ρ_c

4. Results

In order to specify the adequate ranges of temperature and pressure for each pure substance, we fit the individual data groups separately by affecting different values to the coefficients $\{\alpha_K\} = \{\alpha_G, \alpha_L, \alpha_{VLE}, \alpha_V, \alpha_{CP}, \alpha_B\}$ in the expression of the objective function $\Gamma(\mathbf{a}, \lambda)$ (Eq. (15)). For example, if we consider only the gas phase data, the terms ϕ_K, $K \neq G$ are rejected from the objective function Γ by affecting zero to all α_K coefficients except for α_G. The adjustable parameters resulting from the fit with $\{\alpha_K\} = \{1, 0, 0, 0, 0, 0\}$ are then used to calculate the gas phase properties which are then compared to their data values [3]. Similarly are treated the homogeneous liquid phase and the vapour–liquid equilibrium, with $\{\alpha_K\} = \{0, 1, 0, 0, 0, 0\}$ and $\{\alpha_K\} = \{0, 0, 1, 0, 0, 0\}$, respectively. The results obtained for the considered substances show a satisfactory description of the state behaviour ($\rho - P - T$) in the homogeneous fluid regions as well as at the vapour–liquid equilibrium in the specific ranges of temperature and pressure (Tables 6–14). Several combinations of data groups are considered with various vectors $\{\alpha_K\}$. We can so investigate the influence of fitting with an individual data group or a combination of data groups on the properties of the others as well as test if the incorporation of the considered data set into the calculation is necessary for a reliable Bender equation.

The deviations of calculated properties from their data values are expressed by means of the root of the standard deviation $RAAD_r$ and AAD, defined for a property θ as

$$RAAD_r/\% = \frac{100}{N} \sum_{i=1}^{N} |(\theta - \theta_{cal})/\theta|_i \tag{21}$$

$$AAD = \frac{1}{N} \sum_{i=1}^{N} |\theta - \theta_{cal}|_i \tag{22}$$

where N is the number of data points.

In the following, we will discuss in detail the case of nitrogen as illustration of the procedure adopted. For the rest of the considered fluids, we just present the resulting parameters a_i for the general fit with $\{\alpha_K\} = \{1, 1, 1, 1, 1, 1\}$ as well as the corresponding $RAAD_r$ and AAD (Tables 6–14). An analytical estimation of the standard error as well as the confidence intervals of each parameter in the case of nitrogen for the fit of single phase gas ($\alpha = \{1, 0, 0, 0, 0, 0\}$), shows that at the most two figures of each parameter are significant (Table 4). Through this study, approximative compact list of fitting parameters is given for each considered substance (Tables 5–14). As shown in Tables 6–14, the use of the new compact list does not affect the predictive quality of the volumetric properties.

4.1. Correlations of data groups for nitrogen

Table 3 is structured into several items, where selected combinations of data groups for various vectors α, $K =$

Table 6
Parameters of the Bender EOS and statistical characteristics for argon for the fit with $\{\alpha_K\} = \{1, 1, 1, 1, 1\}$

Parameters	
$a_1 = 5.1106 \times 10^{-3}$, $a_2 = -1.2870$, $a_3 = -3.3752 \times 10^{2}$, $a_4 = 5.2246 \times 10^{3}$, $a_5 = -1.5031 \times 10^{5}$	$a_{11} = 5.5901 \times 10^{-12}$, $a_{12} = -3.1318 \times 10^{-9}$, $a_{13} = 1.5332 \times 10^{-12}$, $a_{14} = 1.0057 \times 10^{2}$, $a_{15} = -2.1466 \times 10^{4}$
$a_6 = 6.7915 \times 10^{-6}$, $a_7 = -1.5428 \times 10^{-3}$, $a_8 = 0.1344$, $a_9 = -1.7997 \times 10^{-9}$, $a_{10} = 2.3236 \times 10^{-6}$	$a_{16} = 1.1965 \times 10^{6}$, $a_{17} = -4.3144 \times 10^{-4}$, $a_{18} = 0.1222$, $a_{19} = -6.3172$, $a_{20} = 5.356 \times 10^{2}$
Statistical characteristics	
G-data	$w_G = 1.0$, $\partial_r Z = 0.31\%$, $\partial Z = 0.003$
L-data	$w_L = 10.92$, $\partial_r Z = 0.44\%$, $\partial Z = 0.002$
V-data	$w_V = 28.67$, $\partial_r B_V = 12.68\%$, $\partial B_V = 0.002$
VLE-data	$w_{VLE} = 105.41$, $\partial_r P_L = 1.3\%$, $\partial_r P_G = 0.17\%$, $\partial_r \rho_{sat}^{(L)} = 0.17\%$, $\partial_r \rho_{sat}^{(G)} = 0.96\%$

Table 7
Parameters of the Bender EOS and statistical characteristics for methane for the fit with $\{\alpha_K\} = \{1, 1, 1, 1, 1\}$

Parameters	
$a_1 = 1.9019 \times 10^{-2}$, $a_2 = -6.5728$, $a_3 = -1.5739 \times 10^{3}$, $a_4 = 2.1534 \times 10^{3}$, $a_5 = 1.4211 \times 10^{5}$	$a_{11} = 6.7980 \times 10^{-10}$, $a_{12} = -5.5187 \times 10^{-7}$, $a_{13} = 8.3738 \times 10^{-10}$, $a_{14} = 9.0544 \times 10^{2}$, $a_{15} = -1.8231 \times 10^{5}$
$a_6 = 6.5279 \times 10^{-5}$, $a_7 = -1.9498 \times 10^{-2}$, $a_8 = 2.4709$, $a_9 = -6.2110 \times 10^{-8}$, $a_{10} = 1.2398 \times 10^{-4}$	$a_{16} = 1.4017 \times 10^{7}$, $a_{17} = -4.9113 \times 10^{-2}$, $a_{18} = 2.0014 \times 10^{1}$, $a_{19} = -1.2579 \times 10^{3}$, $a_{20} = 1.6266 \times 10^{2}$
Statistical characteristics	
G-data, $w_G = 1.0$	$\partial_r Z = 0.21\%$, $\partial Z = 0.002$
L-data, $w_L = 3.26$	$\partial_r Z = 0.33\%$, $\partial Z = 0.003$
V-data, $w_V = 15.14$	$\partial_r B_V = 8.03\%$, $\partial B_V = 0.001$
VLE-data	$w_{VLE} = 35.58$, $\partial_r P_L = 0.56\%$, $\partial_r P_G = 0.13\%$, $\partial_r \rho_{sat}^{(L)} = 0.16\%$, $\partial_r \rho_{sat}^{(G)} = 0.97\%$

Table 8
Parameters of the Bender EOS and statistical characteristics for ethane for the fit with $\{\alpha_K\} = \{1, 1, 1, 1, 1\}$

Parameters	
$a_1 = 2.2048 \times 10^{-2}$, $a_2 = -14.8680$, $a_3 = -4.9390 \times 10^{2}$, $a_4 = -5.6568 \times 10^{5}$, $a_5 = 3.0515 \times 10^{7}$	$a_{11} = 1.2429 \times 10^{-10}$, $a_{12} = -2.8726 \times 10^{-8}$, $a_{13} = 2.4845 \times 10^{-10}$, $a_{14} = 4.1160 \times 10^{2}$, $a_{15} = 5.2327 \times 10^{4}$
$a_6 = 6.9231 \times 10^{-6}$, $a_7 = 1.0396 \times 10^{-2}$, $a_8 = 5.4227$, $a_9 = 1.6384 \times 10^{-7}$, $a_{10} = -1.02 \times 10^{-4}$	$a_{16} = -6.6722 \times 10^{7}$ $a_{17} = -0.1286$, $a_{18} = 6.3893 \times 10^{1}$, $a_{19} = -3.6942 \times 10^{3}$, $a_{20} = 2.070 \times 10^{2}$
Statistical characteristics	
G-data	$w_G = 1.0$, $\partial_r Z = 0.54\%$, $\partial Z = 0.005$
L-data	$w_L = 3.27$, $\partial_r Z = 0.26\%$, $\partial Z = 0.002$
V-data	$w_V = 13.72$, $\partial_r B_V = 3.04\%$, $\partial B_V = 0.001$
VLE-data	$w_{VLE} = 39.88$, $\partial_r P_L = 0.77\%$, $\partial_r P_G = 0.14\%$, $\partial_r \rho_{sat}^{(L)} = 0.09\%$, $\partial_r \rho_{sat}^{(G)} = 0.58\%$

Table 9
Parameters of the Bender EOS and statistical characteristics for krypton for the fit with $\{\alpha_K\} = \{1, 1, 1, 1, 1\}$

Parameters	
$a_1 = 3.1860 \times 10^{-3}$, $a_2 = -1.3887$, $a_3 = -2.4604 \times 10^{2}$, $a_4 = -1.1092 \times 10^{4}$, $a_5 = 3.8876 \times 10^{5}$	$a_{11} = 4.9629 \times 10^{-13}$, $a_{12} = -4.0074 \times 10^{-10}$, $a_{13} = 1.4205 \times 10^{-13}$, $a_{14} = 2.2258 \times 10^{1}$, $a_{15} = -1.9302 \times 10^{3}$
$a_6 = 1.5687 \times 10^{-6}$, $a_7 = -3.0953 \times 10^{-4}$, $a_8 = 0.1022$, $a_9 = 4.5100 \times 10^{-10}$, $a_{10} = 1.7482 \times 10^{-7}$	$a_{16} = -5.2138 \times 10^{5}$, $a_{17} = -1.0767 \times 10^{-4}$, $a_{18} = 3.4194 \times 10^{-2}$, $a_{19} = -1.1637$, $a_{20} = 9.084 \times 10^{2}$
Statistical characteristics	
G-data	$w_G = 1.0$, $\partial_r Z = 0.31\%$, $\partial Z = 0.003$
L-data	$w_L = 8.85$, $\partial_r Z = 0.36\%$, $\partial Z = 0.002$
V-data	$w_V = 28.23$, $\partial_r B_V = 11.98\%$, $\partial B_V = 0.002$
VLE-data	$w_{VLE} = 84.69$, $\partial_r P_L = 0.85\%$, $\partial_r P_G = 0.06\%$, $\partial_r \rho_{sat}^{(L)} = 0.14\%$, $\partial_r \rho_{sat}^{(G)} = 0.57\%$

Table 10
Parameters of the Bender EOS and statistical characteristics for neon for the fit with $\{\alpha_K\} = \{1, 1, 1, 1, 1, 1\}$

Parameters	
$a_1 = 6.1712 \times 10^{-3}$, $a_2 = -0.2386$, , $a_3 = -7.5748 \times 10^{1}$, $a_4 = 2.2144 \times 10^{3}$, $a_5 = -2.6381 \times 10^{4}$	$a_{11} = 2.201 \times 10^{-12}$, $a_{12} = 6.2366 \times 10^{-10}$, $a_{13} = 2.81 \times 10^{-13}$, $a_{14} = -2.0708 \times 10^{1}$, $a_{15} = 2.0279 \times 10^{3}$
$a_6 = 2.6707 \times 10^{-6}$, $a_7 = 1.0554 \times 10^{-3}$, $a_8 = -7.9161 \times 10^{-3}$, $a_9 = 2.9108 \times 10^{-9}$, $a_{10} = -1.4130 \times 10^{-6}$	$a_{16} = -5.0109 \times 10^{4}$, $a_{17} = 5.6119 \times 10^{-6}$, $a_{18} = -7.6984 \times 10^{-4}$, $a_{19} = 3.0147 \times 10^{-2}$, $a_{20} = 4.8191 \times 10^{2}$
Statistical characteristics	
G-data	$w_G = 1.0$, $\partial_r Z = 0.01\%$, $\partial Z = 0.001$
V-data	$w_V = 27.13$, $\partial_r B_V = 3.47\%$, $\partial B_V = 0.000$

Table 11
Parameters of the Bender EOS and statistical characteristics for nitrogen for the fit with $\{\alpha_K\} = \{1, 1, 1, 1, 1, 1\}$

Parameters	
$a_1 = 1.0809 \times 10^{-2}$, $a_2 = -2.6663$, $a_3 = -2.6713 \times 10^{2}$, $a_4 = -6.0196 \times 10^{3}$, $a_5 = 1.7340 \times 10^{5}$	$a_{11} = 3.7714 \times 10^{-11}$, $a_{12} = -1.8692 \times 10^{-8}$, $a_{13} = 1.7616 \times 10^{-11}$, $a_{14} = 1.4065 \times 10^{2}$, $a_{15} = -2.5755 \times 10^{4}$
$a_6 = 1.5194 \times 10^{-5}$, $a_7 = -2.7664 \times 10^{-3}$, $a_8 = 0.2643$, $a_9 = 6.8534 \times 10^{-9}$, $a_{10} = 6.2324 \times 10^{-6}$	$a_{16} = 1.3066 \times 10^{6}$, $a_{17} = -1.6227 \times 10^{-3}$, $a_{18} = 0.4203$, $a_{19} = -1.8948 \times 10^{1}$, $a_{20} = 3.1330 \times 10^{2}$
Statistical characteristics	
G-data	$w_G = 1.0$, $\partial_r Z = 0.29\%$, $\partial Z = 0.003$
L-data	$w_L = 32.13$, $\partial_r Z = 0.52\%$, $\partial Z = 0.002$
V-data	$w_V = 25.31$, $\partial_r B_V = 5.75\%$, $\partial B_V = 0.001$
VLE-data	$w_{VLE} = 167.74$, $\partial_r P_L = 0.61\%$, $\partial_r P_G = 0.24\%$, $\partial_r \rho_{sat}^{(L)} = 0.12\%$, $\partial_r \rho_{sat}^{(G)} = 0.91\%$

Table 12
Parameters of the Bender EOS and statistical characteristics for xenon for the fit with $\{\alpha_K\} = \{1, 1, 1, 1, 1, 1\}$

Parameters	
$a_1 = 2.5349 \times 10^{-3}$, $a_2 = -1.3864$, $a_3 = -4.9994 \times 10^{2}$, $a_4 = -7.0781 \times 10^{3}$, $a_5 = 5.6026 \times 10^{5}$	$a_{11} = -7.1791 \times 10^{-14}$, $a_{12} = 1.0748 \times 10^{-10}$, $a_{13} = 3.2873 \times 10^{-14}$, $a_{14} = 2.7647 \times 10^{1}$, $a_{15} = 1.3347 \times 10^{3}$
$a_6 = -1.2329 \times 10^{-7}$, $a_7 = 5.9897 \times 10^{-4}$, $a_8 = 0.1013$, $a_9 = 1.3338 \times 10^{-9}$, $a_{10} = -7.7897 \times 10^{-7}$	$a_{16} = -3.9274 \times 10^{6}$, $a_{17} = -1.589 \times 10^{-4}$, $a_{18} = 6.6339 \times 10^{-2}$, $a_{19} = -2.1472$, $a_{20} = 11.00 \times 10^{2}$
Statistical characteristics	
G-data	$w_G = 1.0$, $\partial_r Z = 0.43\%$, $\partial Z = 0.004$
L-data	$w_L = 5.55$, $\partial_r Z = 0.41\%$, $\partial Z = 0.002$
V-data	$w_V = 25.2$, $\partial_r B_V = 5.54\%$, $\partial B_V = 0.002$
VLE-data	$w_{VLE} = 56$, $\partial_r P_L = 0.79\%$, $\partial_r P_G = 0.04\%$, $\partial_r \rho_{sat}^{(L)} = 0.11\%$, $\partial_r \rho_{sat}^{(G)} = 0.55\%$

G, L, VLE, V, CP, B are considered. From the fit with $\alpha = \{1, 0, 0, 0, 0, 0\}$, it is obvious that the volumetric properties (Z, P) for the gas phase are mutually consistent, with an overall $RAAD_r$ lower then 0.06%, but the liquid phase region is not described correctly since the predicted values are more than 100% apart from the data. On the contrary, the use of L-data alone, corresponding to $\alpha = \{0, 1, 0, 0, 0, 0\}$, results in a good description of the liquid phase properties, but leads to significant deviations in the gas phase region with an overall $RAAD_r$ for the compressibility factor Z_G and the pressure P_G higher than 83 and 53%, respectively. When both of these data sets are considered, $\alpha = \{1, 1, 0, 0, 0, 0\}$,

Table 13
Parameters of the Bender EOS and statistical characteristics for oxygen for the fit with $\{\alpha_K\} = \{1, 1, 1, 1, 1, 1\}$

Parameters	
$a_1 = 1.0286 \times 10^{-2}$, $a_2 = -3.735$, $a_3 = -1.5354 \times 10^{2}$, $a_4 = -9.1063 \times 10^{3}$, $a_5 = 2.3839 \times 10^{5}$	$a_{11} = -2.7781 \times 10^{-12}$, $a_{12} = 1.4746 \times 10^{-9}$, $a_{13} = 2.2205 \times 10^{-12}$, $a_{14} = 1.0410 \times 10^{2}$, $a_{15} = -2.2781 \times 10^{4}$
$a_6 = -3.5843 \times 10^{-6}$, $a_7 = 2.8114 \times 10^{-3}$, $a_8 = 0.1379$, $a_9 = 2.5432 \times 10^{-8}$, $a_{10} = -6.5938 \times 10^{-6}$	$a_{16} = 1.0584 \times 10^{6}$, $a_{17} = -6.2873 \times 10^{-4}$, $a_{18} = 0.1909$, $a_{19} = -8.5967$, $a_{20} = 4.361 \times 10^{2}$
Statistical characteristics	
G-data	$w_G = 1.0$, $\partial_r Z = 0.22\%$, $\partial Z = 0.002$
L-data	$w_L = 13.38$, $\partial_r Z = 0.66\%$, $\partial Z = 0.004$
V-data	$w_V = 26.04$, $\partial_r B_V = 9.24$, $\partial B_V = 0.001$
VLE-data	$w_{VLE} = 73$, $\partial_r P_L = 1.26\%$, $\partial_r P_G = 0.15\%$, $\partial_r \rho_{sat}^{(L)} = 0.11\%$, $\partial_r \rho_{sat}^{(G)} = 0.71\%$

Table 14
Parameters of the Bender EOS and statistical characteristics for carbon dioxide for the fit with $\{\alpha_K\} = \{1, 1, 1, 1, 1, 1\}$

Parameters	
$a_1 = 9.2695 \times 10^{-3}$, $a_2 = -5.6387$, $a_3 = -3.7608 \times 10^2$, $a_4 = -2.9838 \times 10^5$, $a_5 = 1.4837 \times 10^7$	$a_{11} = 4.9083 \times 10^{-12}$, $a_{12} = -9.2096 \times 10^{-10}$, $a_{13} = 3.7029 \times 10^{-12}$, $a_{14} = -1.7365 \times 10^3$, $a_{15} = 1.1409 \times 10^6$
$a_6 = 4.1742 \times 10^{-6}$, $a_7 = 1.5959 \times 10^{-3}$, $a_8 = 1.1767$, $a_9 = 1.1034 \times 10^{-8}$, $a_{10} = -8.3435 \times 10^{-6}$	$a_{16} = -1.8758 \times 10^8$, $a_{17} = -2.0563 \times 10^{-4}$, $a_{18} = -1.2645$, $a_{19} = 5.3148 \times 10^2$, $a_{20} = 4.676 \times 10^2$
Statistical characteristics	
G-data	$w_G = 1.0$, $\partial_r Z = 0.09\%$, $\partial Z = 0.000$
L-data	$w_L = 12.53$, $\partial_r Z = 0.29\%$, $\partial Z = 0.001$
V-data	$w_V = 31.15$, $\partial_r B_V = 3.01\%$, $\partial B_V = 0.000$
VLE-data	$w_{VLE} = 123.91$, $\partial_r P_L = 0.45\%$, $\partial_r P_G = 0.09\%$, $\partial_r \rho_{sat}^{(L)} = 0.09\%$, $\partial_r \rho_{sat}^{(G)} = 0.17\%$

the liquid and the gas phases are correctly described but the vapour–liquid equilibrium is not accurately predicted, with a relative deviation of about 11%. Similarly, the evaluation of the Bender equation parameters with $\alpha_{VLE} = 1$, results in a good description of the vapour–liquid equilibrium as illustrated in Table 3. The fit with $\alpha = \{1, 1, 1, 0, 0, 0\}$ leads to an overall good agreement with the basic data for the homogeneous phases as well as the saturation properties with an overall $RAAD_r$ ranging from 0.2% to 0.5%. We can then conclude on the necessity of incorporating each data group for the obtention of a reliable equation of state describing accurately the state behaviour of the homogeneous fluid regions as well as the vapour–liquid equilibrium. A good description of the second virial coefficient is obtained from the fit of single phase gas data ($\alpha = \{1, 0, 0, 0, 0, 0\}$), which is not the case of the other combinations of data groups without reference to the second virial coefficients data ($\alpha_V = \alpha_B = 0$). However the inclusion of virial coefficients for the fit with $\alpha = \{1, 1, 1, 1, 0, 1\}$ or $\alpha = \{1, 1, 1, 1, 1, 1\}$ leads to improved description of this property with an overall $RAAD_r$ ranging from 4.5% to 5.7%. Large deviation at the critical point is observed ($\partial_r Z_c = 30.7\%$) for the fit with $\alpha = \{0, 1, 0, 0, 0, 0\}$. On the other hand, the inclusion of the coordinates of the critical point with $\alpha_{CP} = 1$ does not affect significantly the predictive capability of the equation for the other data groups but leads to a good description at the critical point. The fit with $\alpha = \{1, 1, 1, 0, 1, 0\}$ leads to a good description of both single phase regions, the vapour–liquid equilibrium and the critical point, with a low relative average deviation (0–0.5%) but the second virial coefficient description is worsened. We see in Table 5 that the parameters a_i obtained from the fit with $\alpha = \{1, 1, 1, 0, 0, 0\}$ do not differ significantly from the fit with inclusion of the coordinates of the critical point. The case of the last data set, the second virial coefficients, is worthy of closer consideration. From Table 3 it is seen that equal good prediction of the *PVT* properties and the critical point are performed with the Bender equation, with reference, $\alpha = \{1, 1, 1, 1, 1, 1\}$, and without reference, $\alpha = \{1, 1, 1, 0, 1, 0\}$, to the second virial coefficients, which is not the case of virial coefficients, with a relative deviation of about 31% for $\alpha_V = \alpha_B = 0$. The real importance of the second virial coefficients data will be shown in the next paragraph by the prediction of the Joule–Thomson inversion curve.

4.2. Joule–Thomson inversion curve from the Bender EOS

The Joule–Thomson inversion curve (JTIC) is the locus of states of the thermodynamic surface where the fluid temperature is invariant upon isenthalpic expansion:

$$(\partial T/\partial P)_H = 0 \tag{23}$$

This criterion can be written in several alternative forms, in particular in the following form suitable for the Bender EOS

$$T_r(\partial Z_r/\partial T_r)_{\rho_r} - \rho_r(\partial Z_r/\partial \rho_r)_{T_r} = 0 \tag{24}$$

JTICs are usually represented in the reduced temperature ($T_r := T/T_c$) and reduced pressure ($P_r := P/P_c$) plane, where T_c and P_c are, respectively, the critical temperature and pressure. The JTIC passes through a maximum pressure at intermediate tempearture and goes to zero at a maximum inversion temperature.

It is known that the prediction of the Joule–Thomson inversion curve constitues a rather severe test of an equation of state.

Fig. 1 shows the nitrogen inversion curves for two selected fits in comparison to published data. Curve c1 results when using all data groups, $\alpha = \{1, 1, 1, 1, 1, 1\}$, while curve c2

Table 15
Characteristics of the Joule–Thomson inversion curve for each considered substance

Fluid	T_r	P_r	$T_{r,max}$
Ar	2.26	11.7373	5.04
CH_4	2.26	11.6574	5.0
C_2H_6	2.16	12.1326	4.72
Kr	2.24	11.5088	5.22
Ne	2.38	11.137	4.9
N_2	2.22	11.5354	4.9
O_2	2.22	11.474	5.1
Xe	2.20	11.3985	5.16
CO_2	1.92	12.4181	4.5

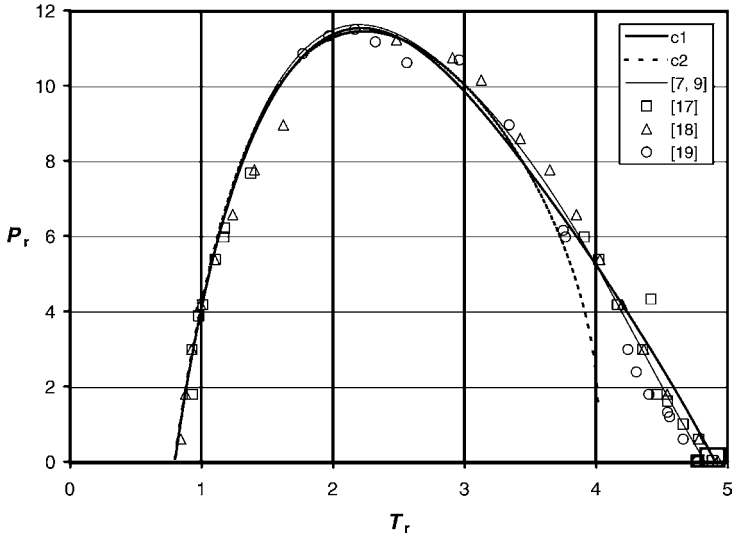

Fig. 1. Comparison between calculated and published inversion data for nitrogen.

is predicted by the fit with $\alpha = \{1, 1, 1, 0, 1, 0\}$ without the second virial coefficients data. Up to $T_r = 3.5$, a good agreement between both curves is observed. But the behaviour of c2 becomes erratic for larger values of the reduced temperature. On the contrary, inversion curve c1 agrees with all the published inversion data [4,9,17–19] of the fluid on the whole reduced temperature range. A good prediction of the $T_{r,\max}$ is also observed.

We have calculated the inversion curves c1 and c2 for all considered fluids and made the same observation: in each case the inversion curve predicted by the Bender equation with reference to the second virial coefficient is more realistic than the one calculated without reference to these data. A further illustration of the good prediction of the inversion curve c1 is seen in Fig. 2 for the case of carbon dioxide. In Table 15 the coordinates of the peak of the inversion curves and the maximum inversion temperature $T_{r,\max}$ as predicted by the Bender equation are given for the considered substances.

5. Correlation of the inversion data of low acentric factor fluids

It is known that the inversion effect obeys the corresponding state principle. In order to establish a corresponding state correlation for the seven low acentric factor fluids considered here (Ar, CH_4, Kr, Ne, N_2, O_2, Xe), we applied the structural optimisation technique developed by Wagner that we implemented earlier [21] in *Mathematica*® (version 4.1). The simple correlation obtained:

$$P_r = 31.541 - 58.389\,e^{-T_r} - 6.194T_r \tag{25}$$

is very similar to the universal equation correlating most of the published inversion data for low acentric factor gases

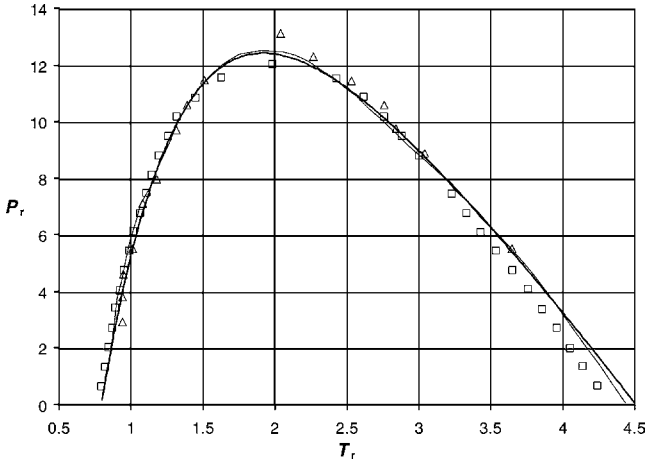

Fig. 2. JTIC of carbon dioxide predicted by: (◯) the Bender EOS; (△) experimental data [20]; (□) compressibility factor [20] and (—) the span Wagner EOS [20].

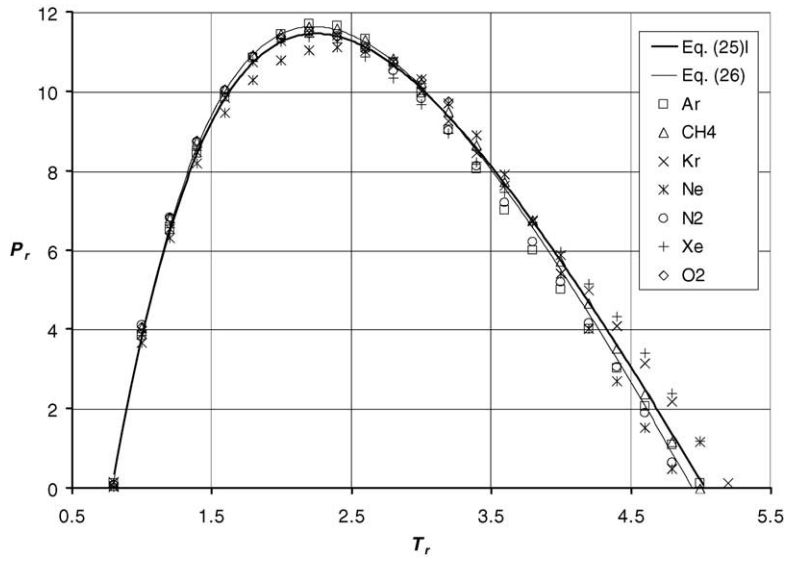

Fig. 3. Comparison between the JTIC predicted by the correlation of Eq. (25) and the published model of Eq. (26) as well as the used data.

established by our research group recently [21]:

$$P_r = 32.771 - 60.859\, e^{-T_r} - 6.535 T_r \quad (26)$$

As shown in Fig. 3, the simple correlation of Eq. (25) describes adequately the used data for the set of considered fluids as well as the inversion data predicted by the model of Eq. (26).

6. Conclusion

The evaluation of the Bender equation parameters yields satisfactory results of the description of the state behaviour of homogeneous fluid regions as well as the vapour–liquid equilibrium curve. The validity of the equation is tested by predicting the Joule–Thomson inversion curve. A substantial result of this study is to show the importance of incorporating a derivative property like the second virial coefficient for the correct evaluation of the EOS parameters. The inversion data predicted by the Bender EOS for several low acentric factor fluids (Ar, CH_4, Kr, Ne, N_2, O_2, Xe) are correlated with a simple model in terms of reduced pressure as a function of reduced temperature.

Nomenclature

a_i	adjustable parameters of the Bender equation
B_V	second virial coefficient
CI	confidence intervals
f	fugacity
H	enthalpy
M	molar mass
N, n	number of values
P	pressure
R	universal gas constant
S	entropy
S.E.	standard error
T	temperature
V	volume
Z	compressibility factor
w	weighing factor

Greek letters

ρ	mass density
Ψ, Γ	objective function
λ	Lagrangian multipliers
∂	partial derivative
ω	acentric factor

Subscripts

B	Boyle
cal	calculated
CP, c	critical point
G, vap	gas phase
L, liq	liquid phase
r	relative
sat	at saturation
VLE	vapour–liquid equilibrium
V	second virial coefficient

Superscripts

cal	calculated
f, L	liquid phase
g, G	gas phase

References

[1] E. Bender, Cryogenics 15 (11) (1975) 667–673.
[2] I. Cibulka, J. Kováčiková, L. Hnědkovský, J.P. Novák, Fluid Phase Equilib. 180 (2001) 27–40.
[3] NIST-Server http://webbook. nist. gov/Chemistry/.
[4] R. Tillner-Roth, Fundamental Equations of State, Shaker Verlag, Aachen, Germany, 1998.
[5] C. Tegler, R. Span, W. Wagner, Eine neue Fundamentalgleichung für das fluide Zustandsgebiet von Argon für Temperaturen von der Schmelzlinie bis 700 K und Drücke bis 1000 MPa, Fortschr. -Ber. VDI Reihe 3, Nr. 480, VDI-Verlag, Düsseldorf, 1997.
[6] U. Setzmann, W. Wagner, J. Phys. Chem. Ref. Data 20 (1991) 1061.
[7] D.G. Friend, H. Ingham, J.F. Ely, J. Phys. Chem. Ref. Data 20 (1991) 275.
[8] R.S. Katti, R.T. Jacobsen, R.B. Stewart, M. Jahangiri, Adv. Cryo. Eng. 31 (1986) 1189.
[9] R.T. Jacobsen, R.B. Stewart, M. Jahangiri, J. Phys. Chem. Ref. Data 15 (1986) 735.
[10] R. Schmidt, W. Wagner, Fluid Phase Equilibria 19 (1985) 175.
[11] R. Span, W. Wagner, J. Phys. Chem. Ref. Data 25 (1996) 1509.
[12] H.V. Kehiaian, Virial coefficients of selected gases, Handbook of Chemistry Physics, CRCnet Base, 1999.
[14] Harwell Subroutine Library, HSL Archive Package, UK.
[15] R. Fletcher, J. Linear Algebra Appl. 14 (3) (1976).
[16] M. Daroux, Analyse Numérique Appliquée, LSGC, ENSIC, Nancy, France, 1991.
[17] R.H. Perry, C.H. Chilton, Chemical Engineer's Handbook, 5th ed., McGraw-Hill, 1973, pp. 82–88.
[18] J.R. Roebuck, H. Osterberg, Phys. Rev. (1934) 46.
[19] W.E. Deming, L.W. Deming, Phys. Rev. 46 (1935) 448.
[20] C.M. Colina, M. Lísal, F.R. Sipersrein, K.E. Gubbins, Fluid Phase Equilib. 202 (2002) 253–262.
[21] K. Fnena, Kh. Mejbri, A. Bellagi, Journal de la société chimique de Tunisie 5 (1) (2003) 95–106.

Further reading

[13] J. Vidal, Thermodynamique: Application au génie chimique et à l'industrie pétrolière, Technip, France, 1997.